Opto-Electronic Advances

Supplementary information

August 2023, Vol. 6, No. 8

DOI: 10.29026/oea.2023.220060

Time-sequential color code division multiplexing holographic display with metasurface

Xin Li[1,2], Qinmiao Chen[3], Xue Zhang[1], Ruizhe Zhao[1], Shumin Xiao[3,4,5]*, Yongtian Wang[1]* and Lingling Huang[1]*

[1]Beijing Engineering Research Center of Mixed Reality and Advanced Display, School of Optics and Photonics, Beijing Institute of Technology, Beijing 100081, China; [2]MoE Key Laboratory of Photoelectronic Imaging Technology and System, and MIIT Key Laboratory of Photonics Information Technology, School of Optics and Photonics, Beijing Institute of Technology, 5 Zhongguancun South Street, Beijing 100081, China; [3]State Key Laboratory on Tunable Laser Technology, Ministry of Industry and Information Technology Key Lab of Micro-Nano Optoelectronic Information System, Harbin Institute of Technology (Shenzhen), Shenzhen 518055, China; [4]National Key Laboratory of Science and Technology on Advanced Composites in Special Environments, Harbin Institute of Technology, Harbin 150080, China; [5]Collaborative Innovation Center of Extreme Optics, Shanxi University, Taiyuan 030006, China.

*Correspondence: SM Xiao, E-mail: shumin.xiao@hit.edu.cn; YT Wang, E-mail: wyt@bit.edu.cn; LL Huang, E-mail: huanglingling@bit.edu.cn

This file includes:

Supplementary information for this paper is available at https://doi.org/10.29026/oea.2023.220060

Section 1: Design of the color CDM computer-generated hologram

A detailed flowchart of the calculation of monochrome computer-generated holograms (CGHs) is shown in Fig. S1. The target images are zero-padded according to the numerical aperture (NA) of the experimental system based on the Fidoc algorithm[S1], where the area limited in the NA is considered as the region of interest; otherwise, it is treated as a do-not-care area, and the origin amplitude distributions are easily obtained from these zero-padded images. Attached with a random initial phase, the wavefront of the images backward propagates to the plane of the CGH, where an inverse Fourier transform (IFT) is employed because the CGHs in our verifications are Fourier holograms. Then, the complex amplitude is divided by the wavefront of the corresponding code reference and weighted and summed together as a complex hologram. This hologram is constrained according to the type of metasurface, which is the kinoform in our verification, and only the phase information is maintained. If the peak signal-to-noise ratio, structural similarity index measure, or other evaluation standards for the encoding process are met, then the constrained CGH is output; otherwise, the CGH should be multiplied by the corresponding code reference to acquire the decoded complex amplitude distribution in each channel on the CGH plane. It is worth noting that if the value of pixels in the code patterns is zero, then a Hadamard product ought to be conducted for these pixels instead of division and multiplication in the decoding and encoding processes, respectively. Subsequently, the decoded complex amplitude is propagated to the imaging plane. An amplitude constraint is applied based on the Fidoc algorithm[S1] and the calculation proceeds to the next iteration. As shown in Fig. 2 and described in the Results section, the CGHs for each color components are directly synthesized as a multiwavelength code division multiplexing (CDM) CGH. This implies that the color components of this CDM CGH are distinct and independent. Hence, CGH is applied as an index for searching the specific size of a particular nanorod from the transmission coefficient dictionary.

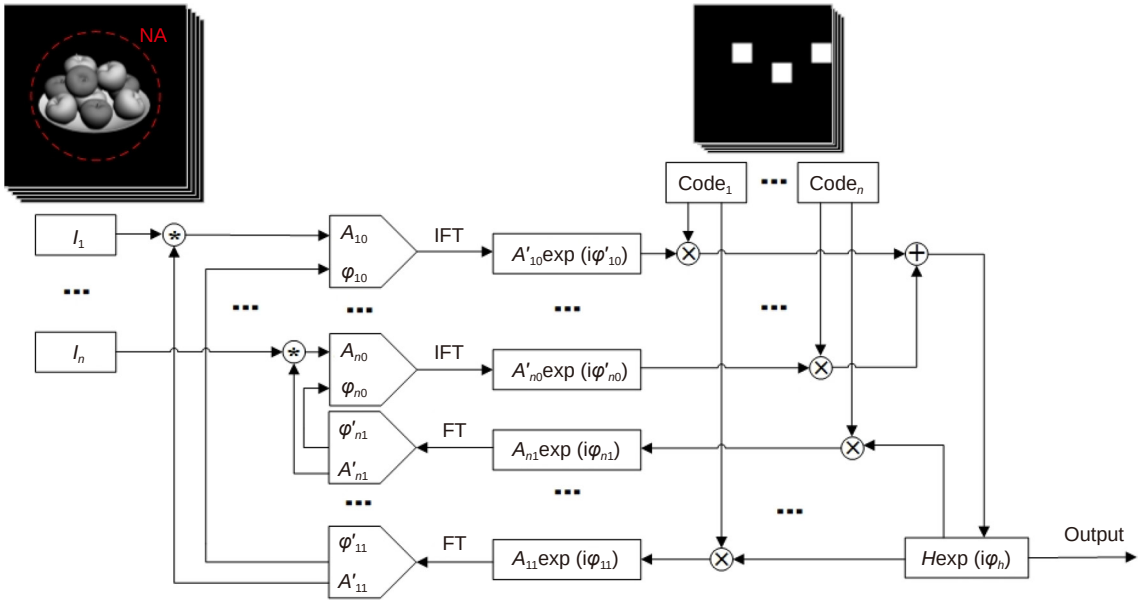

Fig. S1 | Flowchart for the hologram generation in monochrome channel. The hologram is calculated via an iteration optimization, where FT is Fourier transform, IFT represents inverse Fourier transform, ⊙ indicates the amplitude operation according to Fidoc algorithm, ⊗ denotes multiplication, and ⊕ is for superposition with different weights.

Section 2: Code illumination in CDM computer-generated hologram

The experimental results for orthogonal code references are shown in Fig. S2. A series of binary code patterns for each color component were employed in our orthogonal and non- orthogonal verification because precise multilevel amplitude modulation is significantly more difficult to realize in experiments; however, multilevel code patterns are also available for multiwavelength color CDM holography. The simulation results for multilevel patterns at working wavelength of 633 nm are shown in Fig. S3, where the total pixel number of the CGH is 1080×1080 with a pixel pitch of 420 nm, which verifies the feasibility of applying multilevel code patterns in CDM holography. The image quality of the reconstructed results is slightly lower than that of the binary code at a specific wavelength as shown in Fig. S2. The

primary reason is that the code patterns are grey-level images, and they all cover almost the entire hologram, which causes a high overlapping rate for each code pattern. The overlapping area is approximately 99% for each code pattern in this verification with multilevel code patterns, and the intensity proportion in the overlapping area is approximately 34% of the entire pattern. Nevertheless, although the maximum overlapping rate for the verification with binary code patterns for each color component is 67%, the average overlapping rate is only 16% (It is evident from the Fig. 1(a) that there are 5 pure color square blocks that are involved in 2 color code patterns, including 2 square blocks for the same color channel (code1-code3 and code5-code8) and 3 square blocks for different color channels (code1-code8, code1-code4, and code3-code5, as shown in Fig. 2 in this paper)). Conversely, the overlapping exhibits that orthogonality is not strictly followed in code selection and leads to difficulties for eavesdroppers. However, it is worth noting that a higher overlapping rate leads to a higher information density, which directly leads to crosstalk between each code channel because of the limitation of the total information capacity.

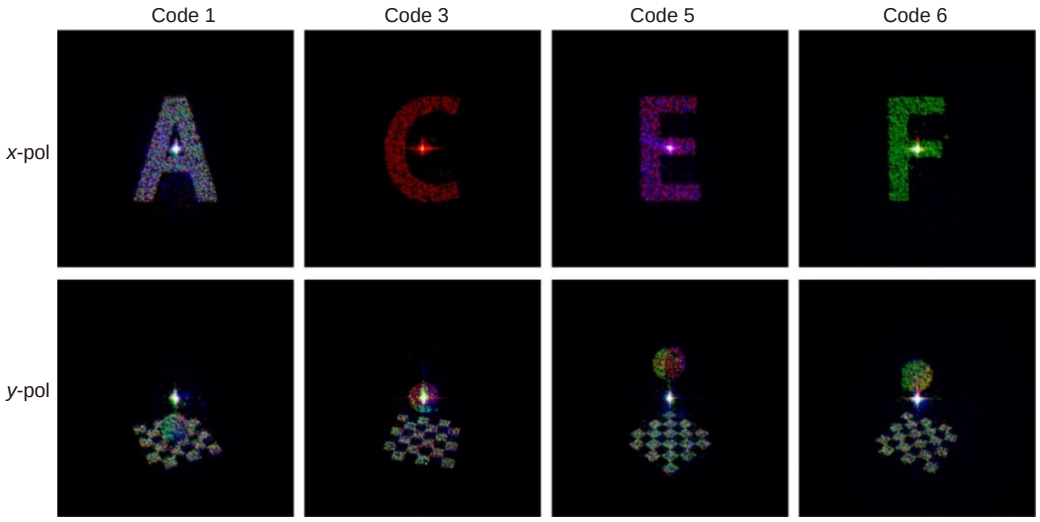

Fig. S2 | Experimental results for orthogonal code references. The images at the first row are reconstructed with horizontal linear polarization state and 4 frames from a video with vertical linear polarization are shown at the second row (see Movie S2).

Only the correct code reference with the correct polarization state leads to target information. As shown in Fig. S4, we performed the experiments with planar illumination. This is due to the fact that all the images were reconstructed and interfered with each other. Eavesdroppers can only decode strong background noise. Moreover, the profile of all images

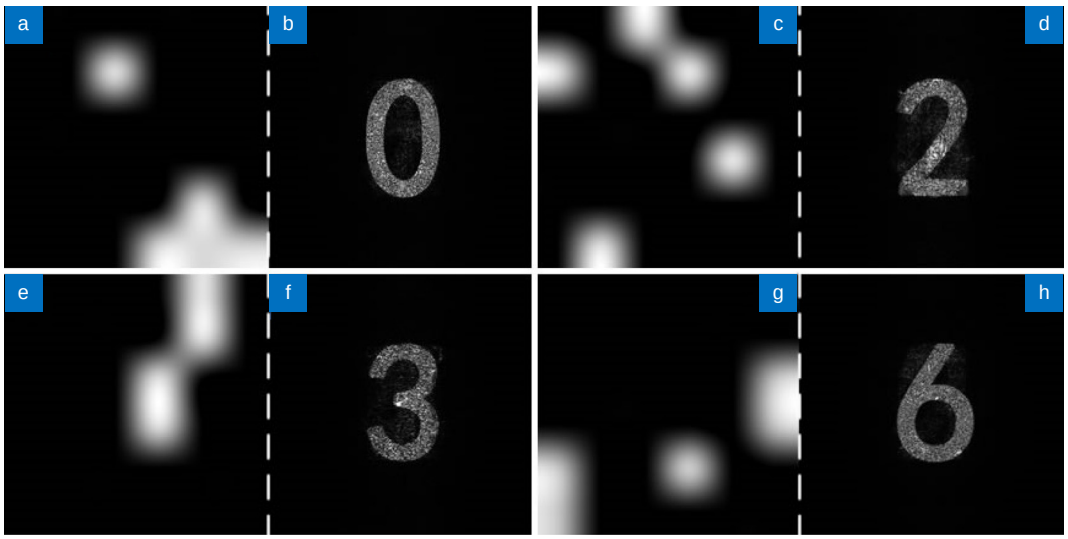

Fig. S3 | Simulation results for multilevel code patterns. (**a**), (**c**), (**e**), and (**g**) are the multilevel code patterns, and (**b**), (**d**), (**f**), and (**h**) are corresponding reconstructed images.

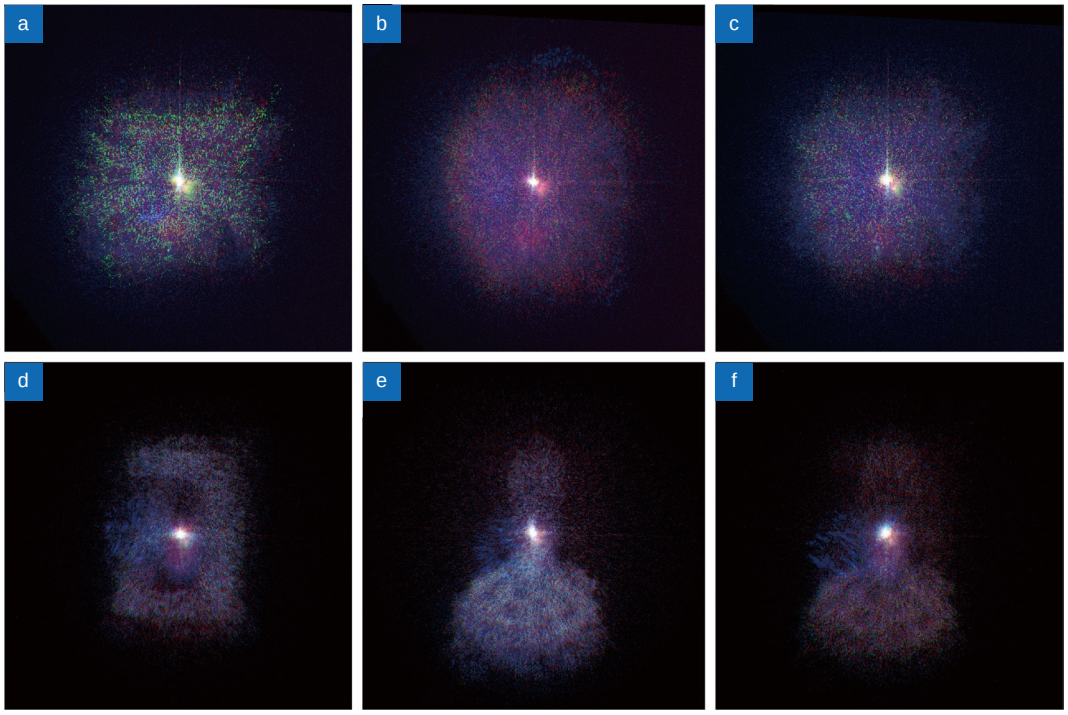

Fig. S4 | Experimental results of planar wave illumination. (**a–c**) The horizontal, vertical, and 45° linear polarization results of sample for the metasurface with nonorthogonal code references. (**d–f**) Corresponding results for the metasurface with orthogonal code references.

reconstructed by the CDM metasurface hologram with orthogonal code reference can be easily learned from Fig. S4(d) and S4(e), but it is difficult to acquire information from images reconstructed by the metasurface hologram with a nonorthogonal code reference as shown in Fig. S4(a) and S4(b). This demonstrates that encoding with a non-orthogonal code reference has higher security because there are more difficulties in cracking the correct code pattern.

Section 3: Transmission efficiency of metasurface

We complete the measurements of the transmission efficiencies of the metasurface recoding the fruit bowl and eight Chinese characters exhibited in the paper, which is encoded with nonorthogonal code references, when the incident light and transmitted light are linearly polarized along the horizontal and vertical directions. At the working wavelengths of 633 nm (R), 532 nm (G), and 460 nm (B), the efficiencies are 35%, 27%, and 36%, respectively, for horizontal linear polarization, and 45%, 33%, and 40%, respectively, for vertical linear polarization. Compared with ideal response of metaatoms in design, such relatively lower efficiencies result from diffusion of kinoform and the mismatch between design and fabrication.

Section 4: Reconstruction qualities of the sample exhibited in the paper

For quantitively evaluating the reconstruction qualities in each code channel, we calculated the peak signal-to-noise ratio (PSNR) and structural similarity (SSIM) of reconstructed image qualities in both code channel and polarization channels according to the calculated multiwavelength CDM CGH response of nanorod shown in Fig. 3. Here, the PSNRs are calculated based on the equation described as

$$PSNR = 10\log_{10}\left(peakval^2/MSE\right) \ , \tag{S1}$$

where *peakval* is the range of the image data, *MSE* is the mean square error between a reconstructed image and the corresponding target image. And the SSIMs are acquired according to

$$SSIM = \frac{\left(2\mu_x\mu_y + C_1\right)\left(2\sigma_{xy} + C_2\right)}{\left(\mu_x^2 + \mu_y^2 + C_1\right)\left(\sigma_x^2 + \sigma_y^2 + C_2\right)} \ , \tag{S2}$$

where μ_x, μ_y, σ_x, σ_y, σ_{xy} are the local means, standard deviations, cross-covariance for images respectively, and $C_1 = (0.01L)^2$,$C_2 = (0.03L)^2$are regularization constants and L is the specified range value of image data. The results are shown in Table 1 and Table 2 for horizontal and vertical polarization channels respectively. Because the eight Chinese diagrams are pure color images then there are some channels have no target information, the PSNRs and SSIMs are not available. As shown in the table, the results have high qualities, which demonstrates the feasibility of our proposed method.

Table S1 | Simulated reconstructed image qualities in horizontal polarization channel.

Code channel		1	2	3	4	5	6	7	8
PSNR	R	NA	25.37	NA	24.28	NA	24.85	32.33	26.31
	G	NA	24.41	24.15	NA	25.12	NA	31.60	25.00
	B	21.43	NA	NA	23.08	23.12	NA	33.17	23.55
SSIM	R	NA	0.97	NA	0.96	NA	0.97	0.98	0.97
	G	NA	0.96	0.95	NA	0.96	NA	0.97	0.96
	B	0.94	NA	NA	0.93	0.95	NA	0.96	0.95

Table S2 | Simulated reconstructed image qualities in vertical polarization channel.

Code channel		1	2	3	4	5	6	7	8
PSNR	R	23.77	25.60	28.44	27.31	27.10	26.12	27.25	26.12
	G	24.17	25.20	27.38	25.94	24.71	25.51	26.91	25.55
	B	28.64	31.81	33.77	27.21	24.25	25.64	31.86	32.41
SSIM	R	0.93	0.94	0.96	0.94	0.94	0.94	0.95	0.94
	G	0.91	0.92	0.95	0.92	0.90	0.91	0.93	0.92
	B	0.97	0.99	0.98	0.93	0.89	0.91	0.97	0.98

Section 5: Details of experiment

We used a supercontinuum laser source (NKT Photonics Superk EVO) to sequentially emit R, G, and B light. A spatial filter, broadband polarizer, and achromatic half-wave plate were utilized to collimate and control the linear polarization state of light. The collimated light was oblique incident on a digital mirror device (DMD), DLP® 6500, at an incident angle of 45° for vertical emergence, where the monochrome code pattern information was synchronously loaded with the corresponding wavelength from the laser source. Before illuminating the metasurface, the light carrying the code information is scaled down via a 4f filtering architecture to match the size of the metasurface and filter out the unwanted high-order diffraction owing to the pixelated structure of the DMD. The reconstructed light was gathered by a 50× objective lens with a numerical aperture of 0.6 and finally imaged on a scientific camera (Thorlabs 1501C-USB) after passing through a broadband analyzer. During the verifications, the light source and DMD were synchronized to ensure that the code patterns corresponded to each color channel.

Section 6: Fabrication of the metasurfaces

Titanium dioxide (TiO_2) film was deposited via electron beam evaporation with a deposition rate of 0.65 Å/s (1 Å=0.1 nm). Subsequently, the sample was fabricated on a 600-nm thick TiO_2 film on an ITO-coated glass substrate. First, the PMMA A2 resist layer was spin-coated on the TiO_2 film. Then, the sample was exposed in the EBL and patterns were developed in MIBK/IPA. Furthermore, a 23 nm thick Cr layer was deposited as a hard mask on the nanopatterns via an electron-gun evaporator, and the lift-off process was performed in the PG remover solution. Subsequently, the designed patterns were transferred to the TiO_2 film by reactive ion etching (RIE). The final sample was obtained by removing the Cr hard mask with a chromium etchant.

Section 7: Recorded videos by changing the code pattern sequentially

Movie S1: Results of two polarization channels for a metasurface with nonorthogonal code references.

Movie S2: Results of two polarization channels for metasurface with orthogonal code references.
They were captured by the Thorlabs CCD, and the white arrows denote the linear polarization state in the video.

References

S1. Georgiou A, Christmas J, Collings N, Moore J, Crossland WA. Aspects of hologram calculation for video frames. *J Opt A Pure Appl Opt* **10**, 035302 (2008).